Structure and timing of transpressional deformation in the Shackleton Glacier area, Ross Orogen, Antarctica

Article *in* Journal of the Geological Society · December 2004

DOI: 10.1144/0016-764903-040

CITATIONS
21

READS
204

3 authors:

Timothy Paulsen
University of Wisconsin - Oshkosh
107 PUBLICATIONS **2,614** CITATIONS
SEE PROFILE

John Encarnación
Saint Louis University
53 PUBLICATIONS **1,441** CITATIONS
SEE PROFILE

Anne Grunow
The Ohio State University
55 PUBLICATIONS **1,989** CITATIONS
SEE PROFILE

Journal of the Geological Society, London, Vol. **161**, 2004, pp. 1027–1038. Printed in Great Britain.

Structure and timing of transpressional deformation in the Shackleton Glacier area, Ross orogen, Antarctica

T. S. PAULSEN[1], J. ENCARNACIÓN[2] & A. M. GRUNOW[3]

[1]*Department of Geology, University of Wisconsin, Oshkosh, WI 54901, USA (e-mail: paulsen@uwosh.edu)*

[2]*Department of Earth and Atmospheric Sciences, St. Louis University, 329 Macelwane Hall, 3507 Laclede Ave., St. Louis, MO 63103, USA*

[3]*Byrd Polar Research Center, The Ohio State University, 108 Scott Hall, 1090 Carmack Road, Columbus, OH 43210, USA*

Abstract: Basement of the Transantarctic Mountains comprises the Ross orogenic belt, a Neoproterozoic to Ordovician mobile belt located along the palaeo-Pacific margin of Gondwana. Our structural analysis of deformation in the Liv Group, a sequence of Cambrian volcanic, volcaniclastic, clastic and carbonate rocks, and nearby plutonic rocks indicates that the Shackleton Glacier area has a polyphase deformation history that includes development of both contractional and strike-slip structures. We describe evidence for synchronous contraction and strike-slip movement, and suggest that the structural suite in this area developed, at least in part, within a sinistral transpressive kinematic regime. Deformation in the Shackleton Glacier area is inferred to be at least in part younger than 505 Ma, based on the deformation of the well-dated Taylor Formation. New $^{40}Ar/^{39}Ar$ cooling ages from metamorphosed igneous and sedimentary rocks range from c. 500 to 470 Ma and are interpreted to date orogenic cooling. Based on our structural results, and on consideration of the tectonic environment represented by the Liv Group, we propose that shortening across a subduction-related volcanic arc system caused deformation of the Liv Group and associated plutonic rocks. Oblique convergence and thus, transpression, may have ultimately been related to left-oblique plate subduction.

Keywords: Antarctica, Transantarctic Mountains, Ross orogen, $^{40}Ar/^{39}Ar$, structure.

The Ross orogenic belt in Antarctica represents one of the major mobile belts involved in the Neoproterozoic–early Palaeozoic assembly of Gondwana (Fig. 1; Stump 1992, 1995). Structural, stratigraphic and magmatic assemblages in the Ross orogen are typically viewed as the remnants of a continental arc located along the margin of the East Antarctic craton (Borg *et al*. 1990; Borg & DePaolo 1991; Goodge *et al*. 1993; Stump 1995; Encarnación & Grunow 1996). Although the Ross orogenic belt has been the subject of study for nearly a century, fundamental questions persist about the spatial and temporal patterns of deformation because the remoteness and inaccessibility of the area continues to hamper field study. In this paper, we focus on the kinematics and timing of deformation in the Liv Group and nearby plutonic rocks in the Shackleton Glacier area of the Transantarctic Mountains. We first summarize results from structural study that we use to define the structural and kinematic evolution of the orogen in this area. We then present new $^{40}Ar/^{39}Ar$ cooling ages to constrain the timing of Late Cambrian to Ordovician orogenic cooling. On the basis of our structural and geochronological results, and on consideration of the tectonic setting in which rocks in this area formed, we discuss our results in the context of a tectonic model for deformation in this sector of the orogen.

Geological setting of the Ross orogen

Rocks of the Ross orogen unconformably underlie Devonian–Jurassic sedimentary rocks of the Beacon Supergroup in the Transantarctic Mountains, a major Cenozoic rift flank uplift (Figs 1 and 2; Fitzgerald 1992; Stump 1995; Isbell 1999). In general, structural and geochronological studies indicate that deformation and magmatism varied in space and time in the orogen (Rowell *et al*. 1992, 2001; Goodge *et al*. 1993; Stump 1995; Goodge 1997; Myrow *et al*. 2002; Goodge 2002). Alkaline magmatism commenced in the latest Neoproterozoic and Early Cambrian in southern Victoria Land (Rowell *et al*. 1993; Read & Cooper 1999; Mellish *et al*. 2002), intruding deformed metasedimentary and metavolcanic rocks. Calc-alkaline magmatism was prevalent between *c*. 525 and 480 Ma (Encarnación & Grunow 1996; Allibone & Wysoczanski 2002; Vogel *et al*. 2002). Calc-alkaline granitoids intrude metasedimentary and metaigneous rocks throughout the orogen (i.e. the Granite Harbor intrusive suite), suggesting that orogenesis was related to subduction (Borg *et al*. 1987, 1990; Borg & DePaolo 1991; Stump 1995; Encarnación & Grunow 1996; Rocchi *et al*. 1997). Deformation is documented by geochronology to extend from *c*. 550 Ma to *c*. 480 Ma along the Ross orogen, with most deformation occurring during the Cambrian (Rowell *et al*. 1992, 1993; Stump 1992; Goodge *et al*. 1993; Goodge 1997; Myrow *et al*. 2002). Widespread emplacement of largely undeformed granites occurred after *c*. 500 Ma (Borg *et al*. 1990; Stump 1995; Encarnación & Grunow 1996; Allibone & Wysoczanski 2002). Orogenesis ceased by Late Cambrian to Early Ordovician in most of the orogen, except for the more outboard sector of northern Victoria Land where magmatism and terrane accretion continued until Mid- to Late Devonian (Stump 1995).

Basement geology of the Shackleton Glacier area

The Shackleton Glacier area marks a distinct boundary in the Ross orogen separating different stratigraphic packages and isotopic patterns of plutons. These changes occur across strike of the structural grain. In contrast to the regional structural grain of the Ross orogenic belt, which roughly parallels the trace of the

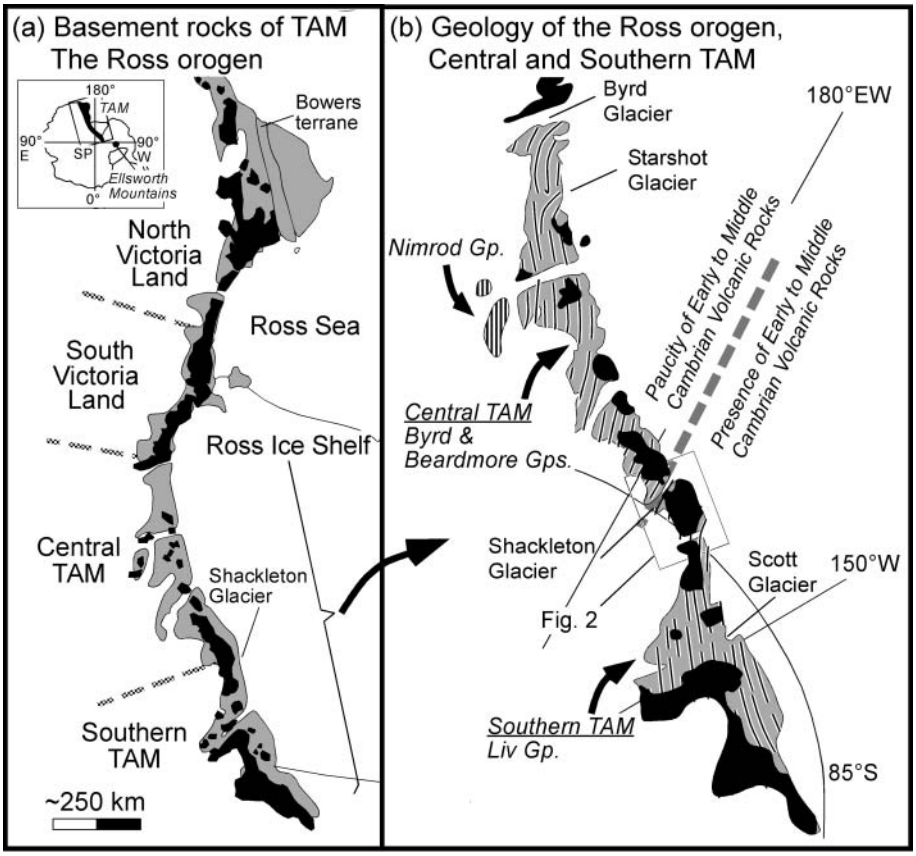

Fig. 1. Simplified geological map of (**a**) basement rocks of the Transantarctic Mountains (TAM; modified from Stump 1992), and (**b**) basement rocks and regional structural trends in the central and southern Transantarctic Mountains. Black regions are exposures of lower Palaeozoic magmatic rocks. Grey areas are exposures of pre-Devonian sedimentary and volcanic rocks that display varying degrees of metamorphism and deformation. Closely spaced vertical stripes are exposures of metamorphic rocks of the Nimrod Group. It should be noted that there are abundant volcanic rocks in Lower to Middle Cambrian stratigraphic packages (i.e. the Liv Group) in the southern TAM, whereas there is a paucity of volcanic rocks in Lower to Middle Cambrian stratigraphic packages (i.e. the Beardmore(?) and Byrd groups) in the central TAM. The boundary (grey dashed line) separating the Liv Group from the Beardmore and Byrd groups occurs west of Shackleton Glacier. The regional structural grain, as defined by bedding strike and fold axis trends, is schematically represented with black lines. It should be noted that the regional structural grain of the Ross orogen displays a number of major map-view curves, particularly at the Shackleton, Starshot and Byrd glaciers. Inset shows locality of Transantarctic Mountains and area of the figure in Antarctica. Geology compiled from Grindley & Laird (1969), McGregor & Wade (1969), Mirsky (1969) and Stump (1992).

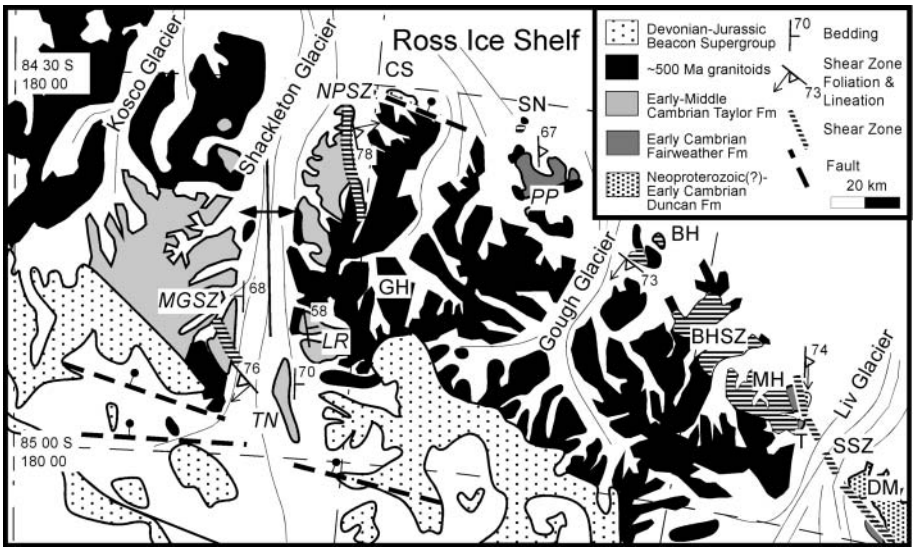

Fig. 2. Simplified map showing the geology of the Shackleton Glacier area (modified from Mirsky 1969). BH, Bravo Hills; BHSZ, Bravo Hills shear zone; CS, Cape Surprise; DM, Duncan Mountains; GH, Gabbro Hills; LR, Lubbock Ridge; MGSZ, Mt. Greenlee shear zone; MH, Mt. Henson; NPSZ, Nilsen Peak shear zone; PP, Polaris Peak; SN, Sage Nunataks; SSZ, Spillway shear zone; TN, Taylor Nunatak; T, the Tusk.

Transantarctic Mountains (Fig. 1), shear zones and folds in the Shackleton Glacier area trend north to NW, at a high angle to the Transantarctic Mountain Front (Fig. 1). West of Shackleton and Kosco glaciers, Lower to Middle Cambrian sedimentary successions in the central Transantarctic Mountains (i.e. the Beardmore(?) and Byrd groups) are largely devoid of volcanic rocks (Rowell & Rees 1989; Myrow *et al*. 2002). By contrast, to the south and east of Shackleton and Kosco glaciers, Lower to Middle Cambrian sedimentary successions in the southern Transantarctic Mountains contain abundant volcanic and volcaniclastic rocks (i.e. the Liv Group; Rowell & Rees 1989; Rowell *et al*. 1997; Wareham *et al*. 2001). The boundary between these different successions is located west of Shackleton Glacier, but is invaded by plutons and obscured by ice and snow. Isotopic patterns of plutons also show marked differences across this boundary and are interpreted to represent contrasting basement age provinces (Borg *et al*. 1990; Borg & DePaolo 1991, 1994). We focused our efforts on the area just east of this boundary in the sedimentary–volcanic succession near Shackleton Glacier.

Previous workers defined four principal stratigraphic units in the Shackleton Glacier area: the Taylor, Greenlee, Fairweather and Duncan formations (Fig. 2; McGregor 1965; Wade *et al*.

1965; Stump 1974, 1985; Wade 1974; Wade & Cathey 1985). Sedimentary and volcanic rocks of the Taylor, Greenlee and Fairweather formations make up the Liv Group (Stump 1982). The Taylor Formation at Taylor Nunatak is the least metamorphosed formation in the Liv Group, being sub-greenschist to greenschist facies, whereas the Greenlee, Fairweather and Duncan formations all experienced greenschist- to amphibolite-facies metamorphism. All of these units exhibit varying degrees of ductile folding and shearing.

The Taylor Formation contains a highly varied assemblage of meta-rhyolitic, -basaltic and -volcaniclastic rocks, limestones, argillites and quartzites (Stump 1982, 1985). Recent U–Pb dates and palaeontological data from felsic volcanic rocks at Lubbock Ridge and carbonate units interbedded with volcanic rocks at Taylor Nunatak, respectively, indicate that the Taylor Formation is Early to Mid-Cambrian in age (516 ± 6 Ma at Lubbock Ridge and 505 ± 1.5 Ma at Taylor Nunatak; Van Schmus *et al*. 1997; Encarnación *et al*. 1999). The Greenlee Formation is stratigraphically below the Taylor Formation and consists of phyllites and quartzites. The Fairweather Formation, which is exposed to the east of Shackleton Glacier near Polaris Peak, contains a highly varied assemblage of marbles (i.e. the Henson Marble Member), meta-rhyolites and quartzites (Stump 1982, 1985; Grunow *et al*. 1996; Rowell *et al*. 1997). Van Schmus *et al*. (1997) reported an age of 550 ± 15 Ma from volcanic rocks of the Fairweather Formation. An Early Cambrian age for the Henson Marble Member of the Fairweather Formation is suggested by probable archaeocyathans (Grunow *et al*. 1996). In the Liv Glacier area, the Spillway Fault juxtaposes the Fairweather Formation with the Duncan Formation, a sequence of quartzites and phyllites of unknown age (Stump 1981). Stump (1985) reported reverse-sense shear indicators where the Spillway Fault places the Duncan Formation on top of the Fairweather Formation and thus, the Duncan Formation is probably older than the Fairweather Formation.

Granitoid plutons of the Granite Harbor intrusive suite intrude all of the pre-Beacon stratigraphic units in the Shackleton Glacier area (Fig. 2). McGregor (1965) classified intrusions as pretectonic and post-tectonic, based on the presence or absence, respectively, of secondary foliations interpreted as having formed during deformation associated with tectonism. Deformed plutonic rocks are exposed along a NW-trending belt herein referred to as the Bravo Hills shear zone (McGregor 1965). Undeformed gabbroic rocks in the Gabbro Hills yielded two-point Sm–Nd mineral isochron ages of 503 and 501 Ma (DePaolo 1996), and are considered to be the oldest undeformed intrusions in the region (Borg *et al*. 1990).

Structure of the Shackleton Glacier area

The Shackleton Glacier area possesses a strong north- to NW-trending structural grain that is defined by the traces of folds, cleavage and shear zones (McGregor 1965; McGregor & Wade 1969; Stump 1985; Wade & Cathey 1985). The following sections outline our structural analysis in the area that extends from the western side of Shackleton Glacier to the western side of Liv Glacier (Fig. 2).

Folds

We recognized two generations of folds (F_1 and F_2) in the study area. F_1 fold axes are generally subhorizontal or plunge moderately to the north or south (Fig. 3a). F_1 fold asymmetries and west-dipping axial planes in the Henson Marble near Polaris Peak indicate east vergence (Figs 3b and 4), whereas F_1 fold asymmetries in the Duncan Mountains indicate SW to west vergence (Stump 1981). F_1 folds were identified in all stratigraphic units in the study area, but are not uniformly developed to the same deformation intensity and style. F_1 folds are common in the Henson Marble where they are characteristically close to isoclinal, with upright to inclined axial planes. We observed mesoscopic boudins on the limbs of F_1 folds in the Henson Marble locally near Polaris Peak and Mt. Henson. Boudins commonly plunge steeply on the limbs of F_1 folds in the Henson Marble with long axes at a high angle to F_1 fold hinges (Figs 3a and 5). Layers are thicker in the hinges, and thinner on the limbs of the F_1 folds. The single dominant F_1 fold in the Taylor Formation is an anticline whose crest is breached and covered by the Shackleton Glacier (Fig. 2; Stump 1985, 1995). Bedding in both limbs of the fold strikes north to NW and dips 45–70°. We observed locally exposed NW-trending mesoscopic F_1 folds in the Taylor Formation at Taylor Nunatak, Nilsen Peak and Mt. Greenlee.

F_2 folds are primarily found within the Henson Marble near

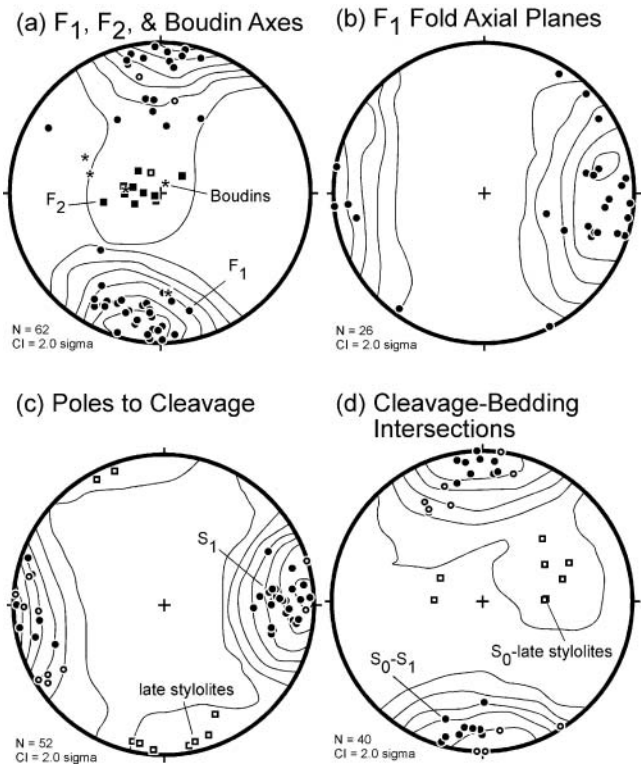

Fig. 3. Synoptic equal-area plots of structural data in the study areas. (**a**) F_1 fold axes (●, Henson Marble; ○, Taylor Formation on Taylor Nunatak), F_2 fold axes (■, Henson Marble; □, Taylor Formation on Taylor Nunatak), and boudin long axes (stars). Kamb contour of F_1 and F_2 fold axes. It should be noted that shallow to moderately plunging F_1 fold axes are distinct from the moderately to steeply plunging F_2 folds. (**b**) F_1 fold axial planes in the Henson Marble. Kamb contour of poles to axial planes. (**c**) Poles to S_1 cleavage (●, Henson Marble; ○, Taylor Formation on Taylor Nunatak) and a late stylolitic cleavage in limestone beds of the Taylor Formation on Taylor Nunatak (□). It should be noted that S_1 cleavage is axial planar to F_1 folds and that the late stylolitic cleavage is at a high angle to the F_1 fold axes. Kamb contour of poles to cleavage. (**d**) S_1 cleavage–bedding (S_0) intersections (●, Henson Marble; ○, Taylor Formation on Taylor Nunatak) and late stylolitic cleavage–bedding (S_0) intersections (□, Taylor Formation on Taylor Nunatak). Kamb contour of intersection lineations.

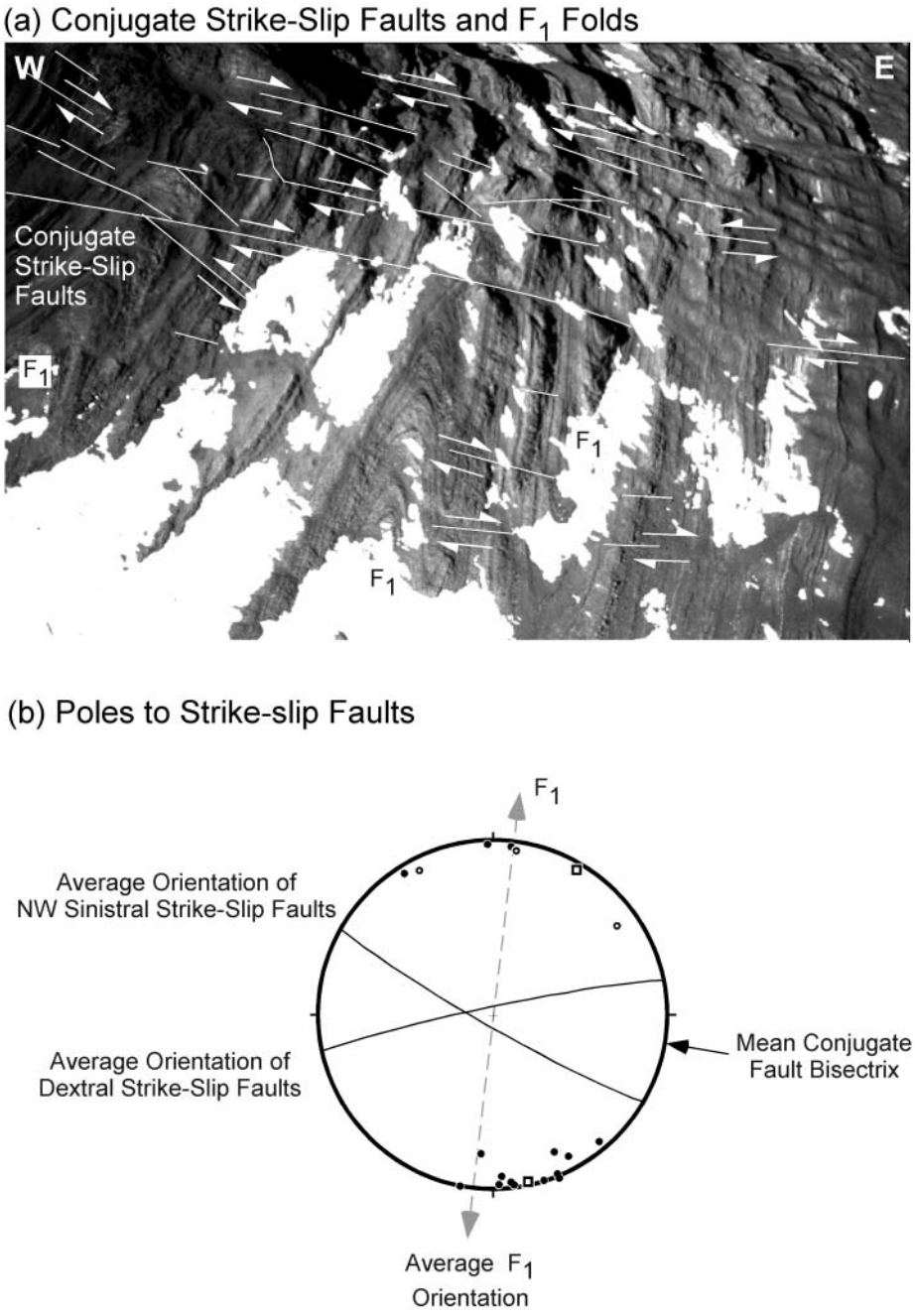

Fig. 4. (**a**) Photograph (oblique aerial view looking north) of north-trending, close to tight F_1 folds in the Henson Marble near Polaris Peak. It should be noted that conjugate strike-slip faults cross-cut F_1 folds at a high angle. Dextral strike-slip faults are more common than sinistral strike-slip faults, a fault pattern that resembles fault arrays that develop by domino-style rotation of fault blocks in response to sinistral shear (Sylvester 1988). Wavelengths of folds in the lower left corner are tens of metres. (**b**) Equal-area plot of strike-slip fault data near Polaris Peak. Dextral strike-slip faults on average strike ENE. Sinistral strike-slip faults range in strike from ENE to WNW, but it is the WNW-striking sinistral strike-slip faults that form a conjugate set to the WSW-striking dextral faults. The average conjugate fault geometry indicates shortening at a high angle to the trend of F_1 fold axes and the strike of S_1 cleavage.

Polaris Peak, the Tusk and Mt. Henson (Fig. 2), where they are developed within the limbs of F_1 folds and possess a moderate to steep plunge (Figs 3a, 5 and 6a, b). We observed one F_2 fold in the Taylor Formation (Fig. 3a). F_2 folds are mesoscopic in scale, deform compositional foliation on the limbs of F_1 folds, and are locally rootless or isoclinal with highly attenuated limbs that locally transpose compositional layering. The asymmetry of F_2 folds indicate sinistral shear (Figs 5 and 6b).

Cleavage

A strong, slaty S_1 disjunctive tectonic cleavage is present in both the Taylor Formation and the Henson Marble, with domain spacing less than 1 mm. S_1 is axial planar to F_1, commonly striking north to NNW, and dipping toward the west (Fig. 3b and c). The lineation, defined by the intersection of S_1 cleavage and bedding, plunges shallowly (i.e. 0–25°) north and south. Bedding–S_1 cleavage intersections in the Taylor Formation indicate that the anticline along Shackleton Glacier has a horizontal, north-trending axis (Fig. 3d). A late stylolitic cleavage cross-cuts S_1 cleavage in limestone beds of the Taylor Formation. This cleavage is subvertical and strikes east–west at a high angle to S_1 cleavage (Fig. 3c). The lineation defined by the intersection of the late stylolitic cleavage and bedding plunges moderately to steeply (i.e. 35–65°) east to ENE and WNW (Fig. 3d).

Ductile shear zones

Shear zones developed within meta-sedimentary, -volcanic and -plutonic rocks and can be identified in the field by the presence

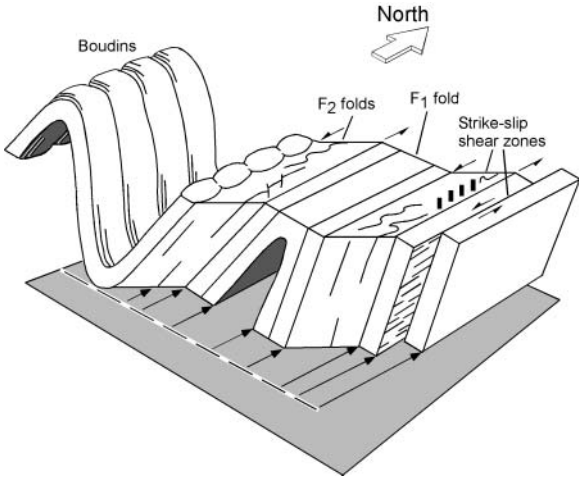

Fig. 5. Schematic diagram illustrating the relationship of F_1 folds to F_2 folds, steeply plunging boudins, and F_1-parallel strike-slip shear zones. Boudins after Price & Cosgrove (1990).

of L–S tectonite fabrics associated with zones of anomalously high strain. The shear zones strike between north and NW (Figs 2 and 7) and can possess dip or along-strike mineral lineations. Dip-slip shear zones are of regional extent and reach kilometre-scale lengths and widths (McGregor 1965; Stump 1981). Strike-slip shear zones are of mesoscopic scale and occur locally, primarily near Polaris Peak, the Tusk and Mt. Henson, but also along shear zones dominated by dip-slip movement (Fig. 2).

Dip-slip shear zones. Four dip-slip shear zones of regional extent are exposed in the Mt. Greenlee and Nilsen Peak areas near Shackleton Glacier, in the Bravo Hills in the Gough Glacier area, and in the Duncan Mountains in the Liv Glacier area (Fig. 2).

The shear zones at Nilsen Peak and at Mt. Greenlee are on the east and west sides of Shackleton Glacier, respectively, where they deform volcanic rocks mapped as Taylor Formation. The shear zones reach lengths of the order of tens of kilometres and widths of the order of 1 km (Fig. 2; McGregor 1965; Stump 1985). The Nilsen Peak shear zone trends north–south and is characterized by a consistently north-striking mylonitic foliation that dips between 75° east and west (Fig. 7a), whereas the Mt. Greenlee shear zone strikes NW and is characterized by a consistently NW-striking mylonitic foliation that dips between 75° NE and SW (Fig. 7b). The shear zones typically have proto- to meso-mylonite textures, and a well-developed foliation. Lineations are defined by elongated quartz (Fig. 8a), strain shadows, and microscopic faulting and boudinage of rigid feldspar grains. In thin section, quartz exhibits undulatory extinction, deformation bands, subgrain development and sutured recrystallized boundaries. Feldspar porphyroclasts show rigid behavior in the form of microfaults and fractures. Collectively, these observations suggest greenschist-facies conditions during deformation

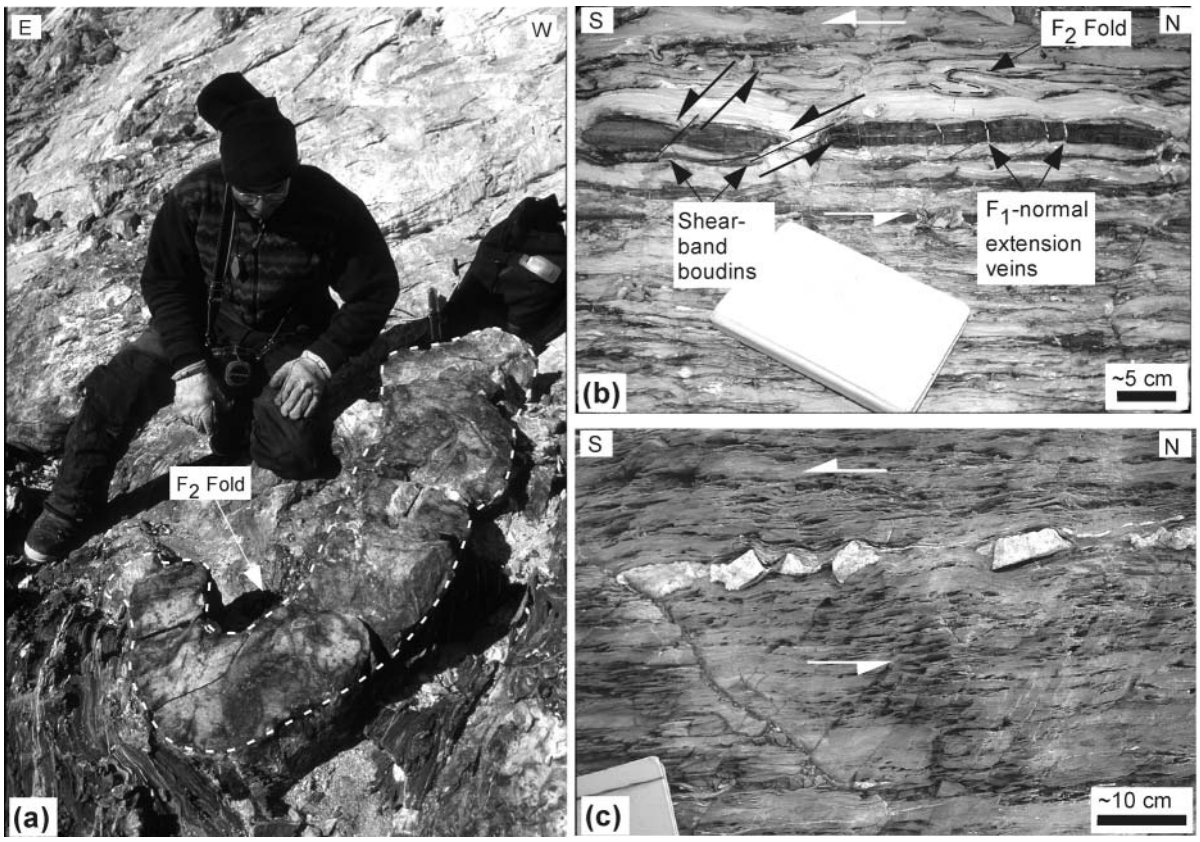

Fig. 6. (**a**) Photograph of steeply plunging, rootless F_2 fold in the Henson Marble at the Tusk near Mt. Henson. (**b**) Photograph of shear-band boudins and a steeply plunging F_2 fold on the limb of an F_1 fold in the Henson Marble near Polaris Peak. It should be noted that the shear-band boudins and F_2 fold indicate sinistral movement within compositional layers; also that F_1-axis parallel extension is indicated by veins located in more competent layers. (**c**) Photograph of rotated boudins in a strike-slip shear zone near Polaris Peak. It should be noted that boudins have been rotated counterclockwise, indicative of sinistral movement parallel to F_1 fold axes.

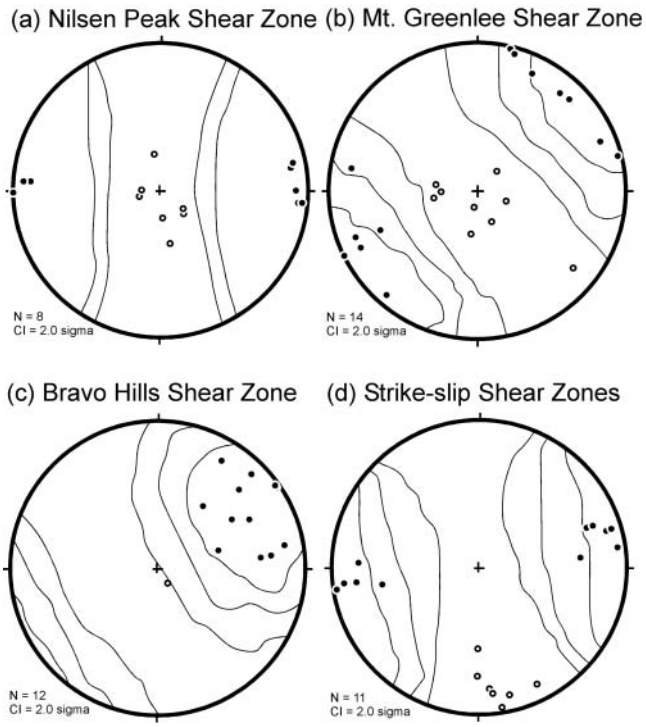

Fig. 7. Synoptic equal-area plots of poles to shear-zone foliation (● and Kamb contour plot) and stretching lineations (○) in shear zones in the study area. It should be noted that the Nilsen Peak (**a**), Mt. Greenlee (**b**) and Bravo Hills (**c**) shear zones are characterized by north- to NW-striking foliations and stretching lineations that plunge steeply in the dip direction of the foliation. By contrast, F_1-parallel strike-slip movement is indicated by shallowly plunging stretching lineations along the Spillway shear zone and other smaller-scale shear zones at the Tusk, Mt. Henson and near Polaris Peak (**d**).

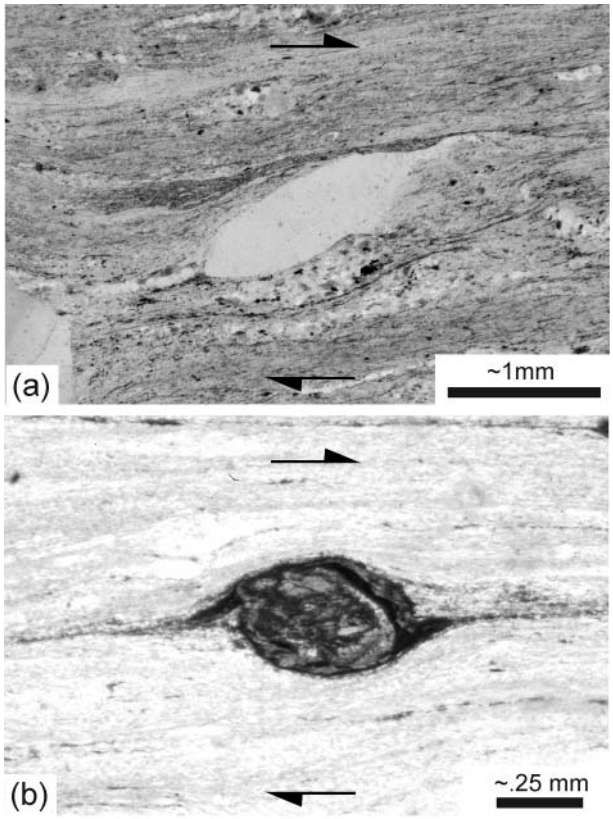

Fig. 8. Photomicrographs of porphyroclasts in the Nilsen Peak shear zone. Sections cut parallel to the stretching lineation and normal to the foliation. (**a**) Sigma-type quartz porphyroclast in the Nilsen Peak shear zone. The stair-stepping displayed by the wings indicates east-side-up movement. (**b**) Delta-type porphyroclast (probably andradite altered to epidote) in the Nilsen Peak shear zone indicative of east-side-up movement in the shear zone.

(Passchier & Trouw 1996). East-side-up shear is indicated in the shear zones by sigma-type porphyroclasts (Fig. 8a), delta-type porphyroclasts (Fig. 8b), asymmetric strain shadows, S–C fabrics and synthetic faults. The overall steep dip of the foliation in these zones (Fig. 7) precludes identification of a hanging wall and footwall, and thus their classification as either reverse or normal-sense shear zones is ambiguous.

We refer to the overall belt of orthogneiss outcrops originally mapped by McGregor (1965) as the Bravo Hills shear zone. McGregor (1965) reported that orthogneiss foliation in the area locally grades laterally into undeformed granodiorite and that the foliation commonly parallels the strike of nearby meta-sediments. Based on mapping by McGregor (1965), the shear zone is *c*. 20 km wide and extends for 75 km from the Bravo Hills to the Mt. Henson area (Fig. 2). We observed orthogneiss that had undergone ductile shearing at multiple localities throughout the Bravo Hills. Here, the shear zone is composed of rocks with dioritic compositions that possess a gneissic foliation defined by alternating leucocratic and mafic laminae. The gneissic foliation strikes NNW and dips 60–85° to the WSW. Rare stretching lineations defined by elongated feldspar plunge steeply down the dip of foliation. Asymmetric mesoscopic NW–NNW-trending F_1 folds locally deform the gneissic foliation and indicate top-to-the-NE (reverse) movement within the shear zone.

In the Liv Glacier area, the Spillway shear zone (i.e. Spillway fault; Stump 1981) juxtaposes the Duncan and Fairweather formations (Fig. 2) and extends for *c*. 45 km from the Duncan Mountains to Mt. Henson. On the SE side of Liv Glacier, the shear zone strikes NW, dips *c*. 75° to the NE, and places the Duncan Formation on top of the Fairweather Formation (Stump 1981). McGregor (1965) and Stump (1981) interpreted overturned and asymmetric, mesoscopic, shallow NW-plunging folds (i.e. F_1 folds) to imply a top-to-the-SW shear direction on the Spillway shear zone within the Duncan Mountains. We examined the shear zone at Mt. Henson on the NW side of Liv Glacier (Fig. 2). Here, the shear zone strikes NNW, dips steeply to the ESE, and juxtaposes the Duncan Formation against a tight, steeply inclined F_1 synform of the Henson Marble Member of the Fairweather Formation (Stump 1981). To the north of Mt. Henson, the shear zone changes dip direction to the NW as observed by Stump (1981).

Strike-slip shear zones. We observed mesoscopic-scale strike-slip shear zones locally, primarily near Polaris Peak, the Tusk and Mt. Henson, but also along shear zones dominated by dip-slip movement (i.e. the Mt. Greenlee and Spillway shear zones). Strike-slip shear zones range from one to tens of metres in length and from 10 cm to a few metres in width. Strike-slip shear zones are located on the limbs of F_1 folds where they strike parallel to compositional layering. F_2 folds related to movement within these zones locally transpose compositional foliation where they are isoclinal. A shallow, south-plunging mineral elongation

defines the stretching lineation. Asymmetric, steeply plunging, F_2 folds (Figs 5 and 6b), together with asymmetric domino-style and shear-band boudins (Fig. 6b and c), suggest that the shear zones typically have a sinistral sense of shear. However, sinistral shear is not ubiquitous in the area. Dextral shear is locally indicated along the Mt. Greenlee shear zone by shear-band boudins. At Sage Nunataks (Fig. 2) shear sense indicators were equivocal; asymmetric steeply plunging mesoscopic folds in white mica schist indicate dextral shear, whereas sinistral shear is indicated by a mesoscopic winged diorite inclusion within orthogneiss.

Faults

A population of strike-slip faults offsets compositional layering in the Henson Marble north of Polaris Peak (Figs 2 and 4). The fault population is formed of subvertical sinistral and dextral strike-slip faults (Fig. 4). As illustrated in Figure 4, dextral strike-slip faults are more common than sinistral strike-slip faults; dextral and sinistral strike-slip faults compose about 75% and 25% of the faults, respectively. The faults display offsets ranging from one to tens of metres and locally have breccias cemented by blocky calcite spar along their traces. Dextral strike-slip faults on average strike WSW, whereas sinistral strike-slip faults range in strike from WNW to WSW. Figure 4a illustrates that the WNW-striking sinistral strike-slip faults form a conjugate fault set to the WSW-striking dextral faults. Our dataset on the orientation of WNW-striking sinistral faults is limited to two data points. The average of these two WNW-striking sinistral faults, along with the average of the dextral faults, indicates that the conjugate fault angle between these sets is *c*. 40°. The conjugate bisector is at a high angle and possibly normal to the trend of F_1 folds (Fig. 4b), consistent with the conjugate faults shown in Figure 5.

Previous workers also identified a number of regional-scale normal faults that displace rocks of the Beacon Supergoup in the area (Fig. 2). Overall, these faults strike WNW parallel to the Transantarctic Mountain Front (Barrett 1965; Mirsky 1969). Recent work in the Cape Surprise area indicates that these WNW faults are dominated by dip-slip, normal-sense movement thought to be related to Transantarctic Mountains uplift (Miller *et al*. 2001). Brittle normal-sense mesoscopic faults in basement rocks in the area may be related to these post-Beacon faults and are not addressed further in this paper.

Relative age of structures

Our structural analysis demonstrates that rocks in the Shackleton Glacier area contain a range of deformation features that include contractional structures (i.e. F_1 folds, S_1 cleavage and reverse-sense shear zones) and strike-slip related structures (i.e. F_1-parallel strike-slip shear zones). The earliest structures identified are north- to NW-trending F_1 folds and S_1 axial planar cleavage, which we denote as D_1. Sinistral strike-slip shear zones and associated F_2 folds formed after F_1 folding, resulting in the refolding and transposition of D_1 fabrics. Steeply plunging boudins formed after F_1 folding, resulting in a deflection of S_1 axial planar cleavage near the necks of boudins. Conjugate strike-slip faults formed after F_1 folding, offsetting F_1 folds and associated cleavage. The conjugate strike-slip faults show brittle deformation (i.e. brecciation) of the ductile fabrics in the Henson Marble, indicating that they probably formed after ductile deformation associated with the sinistral strike-slip shear zones and associated F_2 folds. The late stylolitic cleavage in the Taylor Formation cross-cuts F_1 folds and S_1 cleavage at a high angle, indicating that it postdates the formation of F_1 folds.

Deformation model

Using the cross-cutting structural relationships outlined above, along with a consideration of strain compatibility among structures, we separate the structural evolution of the area into three deformation phases, referred to as D_1, D_2 and D_3 (Fig. 9). D_1 involved the formation of north- to NW-trending F_1 folds, S_1

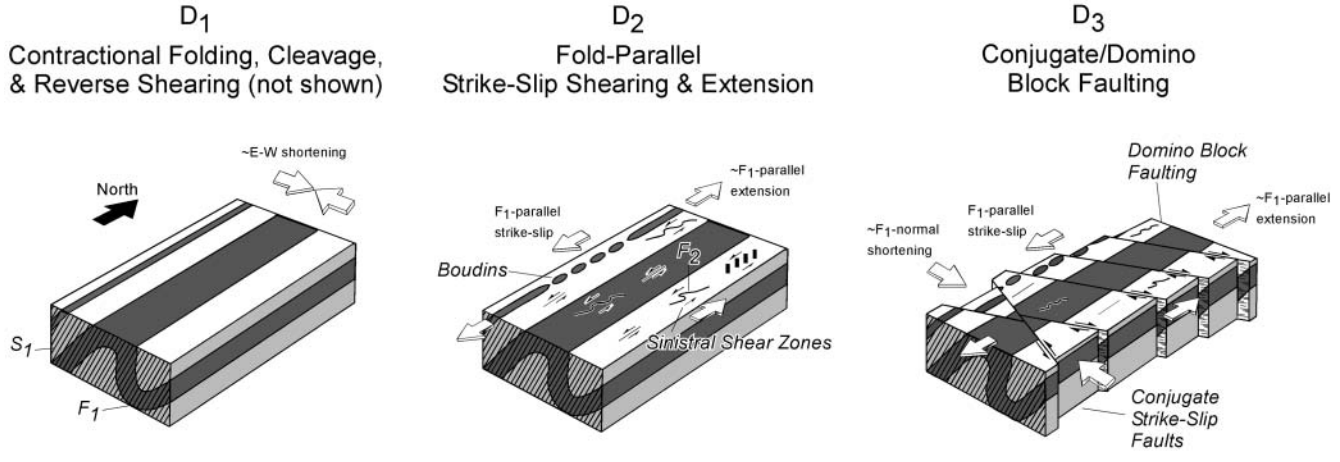

Fig. 9. Schematic model for deformation in the Shackleton Glacier area. F_1 folds, S_1 cleavage, and possibly reverse-sense shear zones formed during the earliest deformation phase, D_1, which was characterized by east–west to NE–SW contraction. Sinistral strike-slip shear zones and steeply plunging boudins formed on the limbs of F_1 folds during the D_2 deformation phase, which was characterized by F_1-parallel sinistral shearing and extension. Conjugate strike-slip faults, with an overall predominance of dextral strike-slip faults, formed during the D_3 deformation phase, which was characterized by coeval approximately F_1-normal shortening, approximately F_1-parallel extension, and F_1-parallel sinistral strike-slip shear (i.e. transpression). By analogy with other transpressive belts, we suggest that the temporal progression of strain from D_1 to D_2 structures (i.e. initial contractional folding followed by fold-parallel strike-slip shearing and extension) collectively reflects a single, progressive, transpressional deformation episode. D_3 conjugate strike-slip faults formed during this transpressional deformation episode, albeit during a later brittle deformation phase.

cleavage, and possibly reverse-sense shear zones (i.e. the Spillway Fault and the Bravo Hills shear zone). D_2 involved the post-F_1 formation of F_2 folds and associated F_1-parallel sinistral strike-slip shear zones, and steeply plunging boudins. D_3 involved the post-F_2 formation of conjugate strike-slip faults at a high angle to F_1 folds and S_1 cleavage.

The orientations of F_1 fold axes and S_1 cleavage indicate that east–west to NE–SW shortening characterized D_1 (Fig. 9). The spatial association of reverse-sense shear zones with F_1 folds, along with their orientation and sense of movement, indicates that they could also have developed during D_1 shortening. The near-vertical orientation of the Nilsen Peak and Mt. Greenlee shear zones precludes their classification as reverse or extensional shear zones. If they are of reverse geometry, then they may also represent D_1 structures. Like previous workers (Stump 1981), we see no evidence for deformation that predates D_1 structures in the area.

F_2 folds and associated strike-slip shear zones, e.g. Polaris Peak, the Tusk and Mt. Henson areas, indicate that D_2 involved sinistral strike-slip shear parallel to F_1 fold axes (Fig. 9). Cross-cutting relations do not constrain the temporal relationship between the sinistral shear zones and the steeply plunging boudins. However, the steeply plunging boudins on the limbs of F_1 folds indicate that F_1-parallel extension and structures indicative of fold-parallel extension and strike-slip shearing could be coeval, as shown in studies of transpressive deformation belts (Kirkwood 1995; Kirkwood *et al*. 1995). Cross-cutting relations also do not constrain the temporal relationship between D_2 structures and reverse-sense dip-slip shear zones, and thus we cannot rule out the possibility that reverse-sense shear zones formed during D_2. A D_2 transpressional strain field would allow for deformation by reverse-sense movement and local evidence for strike-slip movement along the Spillway Fault suggests movement during D_2. If reverse-sense dip-slip shear zones formed coeval with strike-slip shear zones, then strain was partitioned spatially within the orogen, as has been documented in many regions (Platt 1993; Curtis 1997). Local dextral strike-slip movement in the Mt. Greenlee shear zone is hard to relate to D_2 and it therefore may reflect heterogeneous strain or minor strike-slip movement related to lateral F_1-parallel extrusion (e.g. Mancktelow & Pavlis 1994).

The orientation of the D_3 conjugate strike-slip faults, along with their relatively small displacements, represents an infinitesimal strain indicative of synchronous approximately F_1-normal shortening and approximately F_1-parallel extension (Fig. 9). The predominance of dextral strike-slip faults within the overall conjugate array indicates that these faults did not simply form by uniform pure shear. Rather, this pattern resembles fault arrays that facilitate domino-style rotation of fault blocks in response to sinistral shear (Sylvester 1988). The orientation of the dextral strike-slip faults suggests that sinistral shear was oriented roughly parallel to F_1 fold axes. This brittle deformation style would have facilitated attenuation of the deformation zone, which indicates extension approximately parallel to F_1 fold axes. Studies of deformation belts indicate that transpressive deformation, a combination of orthogonal pure shear and simple shear, commonly involves a coeval fold-normal shortening, fold-parallel extension and fold-parallel strike-slip movement (Harland 1971; Sanderson & Marchini 1984; Bürgmann 1991; Kirkwood 1995; Kirkwood *et al*. 1995). The D_3 deformation phase contains all of these characteristics and can therefore be characterized as transpressive.

Our data indicate that a late stylolitic cleavage postdates D_1 structures, but do not constrain the relationship of this cleavage with respect to D_2 or D_3 structures. Given that the late stylolitic cleavage is nonpenetrative, only locally developed and not easily related to any of the deformation phases, it may be related to a younger deformation phase.

Deformation timing

A first approximation of deformation timing in the Shackleton Glacier area is provided by deformation of both the Henson Marble and the Taylor Formation, which have Early Cambrian and Mid-Cambrian (*c*. 505 Ma) depositional ages, respectively (Grunow *et al*. 1996; Encarnación *et al*. 1999). Deformation of these units could be the product of either a single post-505 Ma episode or two distinct episodes, punctuated by deposition of the Taylor Formation. Our structural analysis indicates that D_1 and D_2 structures are present in both units. Furthermore, we saw no evidence for refolded folds or cleavage in the Henson Marble, which could be expected if an earlier deformation episode affected this unit. We therefore favour the simplest scenario with respect to deformational timing, which involves coeval deformation of the units post-505 Ma. Are structural and metamorphic aspects of these units consistent with one deformation episode? D_1 and especially D_2 structures are more common in the Henson Marble than the Taylor Formation; we observed just one F_2 fold in the Taylor Formation. In the context of a single deformation episode, such disparities could reflect differences in the mechanical properties of the units (i.e. rheological strain partitioning) and in their structural level during deformation. Indeed, rocks throughout the area display a higher grade of metamorphism (i.e. greenschist- to amphibolite-facies metamorphism) than do the less metamorphosed greenschist- to sub-greenschist-facies rocks of the Taylor Formation at Taylor Nunatak (Stump 1985, and our own field observations), which could reflect different levels of crustal exposure of the same event. In summary, present geochronological data cannot constrain the exact timing of deformation of the Henson Marble with respect to the Taylor Formation. However, our structural analysis does indicate that D_1 and D_2 structures in the Henson Marble show no discernible difference in orientation from D_1 and D_2 structures in the Taylor Formation, which is consistent with both a single deformation episode or two episodes with similar kinematics.

$^{40}Ar/^{39}Ar$ results

Previous workers have used $^{40}Ar/^{39}Ar$ mineral ages to constrain the timing of orogenic cooling following deformation in the central Ross orogen (Goodge & Dallmeyer 1992, 1996; Baldwin *et al*. 1995; Grunow & Encarnación 2000*a*, *b*). Ductile tectonites in the Nimrod Group (Fig. 1b) have $^{40}Ar/^{39}Ar$ hornblende cooling ages of 524–495 Ma and muscovite cooling ages of 499–496 Ma (Goodge & Dallmeyer 1992, 1996). Granitoids in southern Victoria Land have $^{40}Ar/^{39}Ar$ biotite cooling ages of *c*. 499 ± 3 Ma (Grunow & Encarnación 2000*a*), whereas those in the Scott Glacier area have biotite cooling ages ranging from 496 to 460 Ma (Baldwin *et al*. 1995; Grunow & Encarnación 2000*b*). To constrain the upper age limit of deformation in the Shackleton Glacier area, we conducted an $^{40}Ar/^{39}Ar$ analysis of rocks from the Shackleton Glacier area and adjacent sectors of the range. Analyses were conducted at the Ohio State University $^{40}Ar/^{39}Ar$ geochronology laboratory. For mica samples, around 50 mg of sample were analysed. A larger amount (150 mg) was used for hornblende. Mineral concentrates were obtained by conventional mineral separation techniques and finally hand-picked under a binocular microscope. Argon from the samples was released by

incremental step heating in a resistance furnace prior to mass spectrometric analyses. All $^{40}Ar/^{39}Ar$ mineral ages are corrected with an internal standard calibrated against the standard MMhb1 (Alexander *et al*. 1978) with a nominal age of 523.5 Ma (Renne *et al*. 1994) and are portrayed as age spectra in Figure 10. The analytical data are available from the authors upon request.

Samples GBH-2F6 (hornblende) and GBH-2F5 (white mica) are from schists, whereas samples GBH-2F4 (biotite) and GBH-2F4 (white mica) are from the same hand sample of gneiss. All are from the most SSW nunatak of the Sage Nunataks and are interpreted as deformed plutonic rocks (McGregor 1965; Figs 2 and 10a–d). GBH-2F4 is from the south end of the nunatak. GBH-2F5 and GBH-2F6 were collected a few tens of metres to the north of GBH-2F4. These samples yielded intermediate- to high-temperature plateau ages of 500 ± 5 Ma (hornblende), 484 ± 3 Ma and 489 ± 3 Ma (white mica), and 491 ± 3 Ma (biotite). Samples HEN-4 (white mica) and HEN-10 (phlogopite) are from metasandstones in marbles at Mt. Henson (Figs 2 and 10e, f). These samples yielded intermediate- to high-temperature plateau ages of 475 ± 3 Ma (white mica) and 477 ± 6 Ma (phlogopite). Overall, our results are similar to preliminary $^{40}Ar/^{39}Ar$ mineral ages reported for rocks in the Shackleton Glacier area (Baldwin *et al*. 1999).

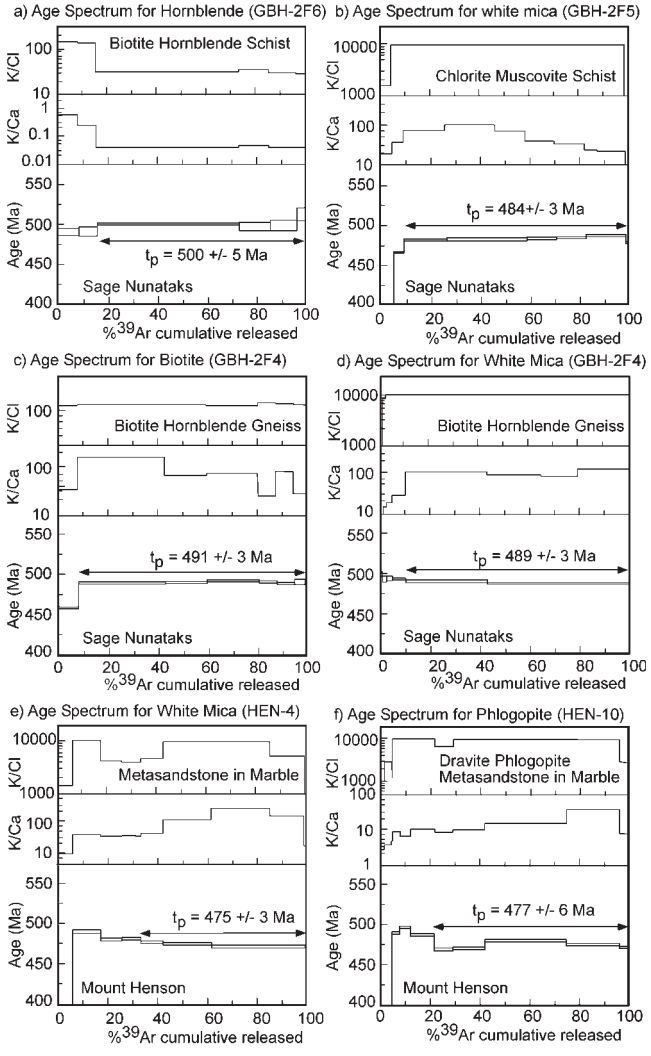

Fig. 10. $^{40}Ar/^{39}Ar$ incremental release spectra for biotite, white mica, phlogopite and hornblende separates from deformed plutonic rocks at Sage Nunataks, and metasandstones in the Henson Marble at Mt. Henson. Samples GBH-2F4 (biotite and white mica) come from the same rock sample. Vertical axes represent age (Ma), and ratios of K/Ca and K/Cl released; horizontal axis is cumulative percent ^{39}Ar released. The thickness of the bars on the age spectrum plots is $\pm 1\sigma$, whereas the uncertainties on the reported plateau ages are $\pm 2\sigma$.

The closure temperature for hornblende (530 ± 30 °C; Harrison 1981) approximates temperatures expected for the amphibolite-grade metamorphism observed in the area (McGregor 1965). The 500 ± 5 Ma $^{40}Ar/^{39}Ar$ hornblende age from Sage Nunataks reflects cooling following metamorphism, and thus represents a minimum deformation age. We interpret the younger white mica ages to date the time of cooling following Ross deformation because the closure temperature for white mica (375 ± 25 °C; Dodson 1979) is lower than the temperatures expected for the metamorphic grade. We also attribute the biotite age from the Sage Nunataks locality to reflect orogenic cooling because the closure temperature for biotite (295–410 ± 50 °C depending on the Fe/Mg ratio; Blanckenburg *et al*. 1989) is lower than the temperatures expected for the metamorphic grade. The biotite plateau age is concordant with the white mica ages within analytical error, which may be due to rapid exhumation or the chemistry of the biotite.

Tectonic synthesis

Geologists have long debated the spatial and temporal patterns of deformation along the Ross orogen. Considerable discussion has revolved around whether the Ross orogen as a whole is a compressive (Kleinschmidt *et al*. 1992; Stump *et al*. 2002) or transpressive orogen (Goodge *et al*. 1993; Jones 1997; Rocchi *et al*. 1997; Cook & Craw 2001). Our results indicate that D_1 structures in the Shackleton Glacier area could have formed during orthogonal convergence. However, compressive orogenic models cannot explain D_2 structures, indicating that deformation involved orogen-parallel strike-slip movement and extension. Compressive orogenic models also cannot explain D_3 structures, indicating that deformation involved components of orogen-normal shortening and orogen-parallel strike-slip movement, which were at least in part synchronous, indicating a transpressive strain field. Can transpressive orogenic models explain D_1 and D_2 structures in the Shackleton Glacier area? Studies of other transpressive belts indicate that deformation commonly involves a temporal progression of strain, with initial folding followed by the development of fold-parallel strike-slip shear zones and structures indicative of fold-axis parallel extension (LaFrance 1989; Kirkwood 1995; Kirkwood *et al*. 1995). The Shackleton Glacier area shows a similar deformation sequence. D_1 produced north- to NW-trending F_1 folds and associated cleavage. As F_1 folds tightened, shear zones and steeply plunging boudins on the limbs of F_1 folds accommodated F_1-parallel sinistral strike-slip movement and extension, respectively. We therefore suggest that D_1 and D_2 structures collectively reflect a single, progressive, transpressional deformation episode, involving kinematic partitioning, with a rheological control on deformation intensity. D_3 conjugate strike-slip faults also formed during this transpressional deformation episode, albeit during a later brittle deformation phase.

The youngest deformed unit in the Shackleton Glacier area is the Taylor Formation (*c*. 505 ± 1.5 Ma; Encarnación *et al*. 1999). Thus, deformation of the Taylor Formation constrains the Ross

orogeny to be Mid-Cambrian or younger in this sector of the orogen, consistent with models of diachronous deformation during the Ross orogeny (Rowell *et al*. 1992; Goodge *et al*. 1993; Goodge 1997; Rowell *et al*. 2001; Myrow *et al*. 2002). In general, the $^{40}Ar/^{39}Ar$ cooling ages indicate closure between about 500 ± 5 Ma (hornblende) and 475 ± 3 Ma (white mica), which we interpret to date orogenic cooling associated with uplift and unroofing of the orogen. These ages are similar to $^{40}Ar/^{39}Ar$ cooling ages reported elsewhere in the Transantarctic Mountains, which generally are in the 490–500 Ma range (Late Cambrian), although some of our Shackleton Glacier area results are slightly younger, yielding Ordovician cooling ages (Goodge & Dallmeyer 1992, 1996; Baldwin *et al*. 1995, 1999; Grunow & Encarnación 2000*a*, *b*; Goodge 2002). The $^{40}Ar/^{39}Ar$ cooling ages from hornblende and muscovite indicate an average post-kinematic cooling rate of *c*. 6 °C Ma^{-1} in the Shackleton Glacier area. To determine an average denudation rate for the area, this cooling rate can be multiplied by an assumed inverse geothermal gradient. Deformation in the Shackleton Glacier area is likely to have occurred in a subduction-related volcanic-arc setting (Borg *et al*. 1990). Thus, if we assume geothermal gradients of 25 °C km^{-1} and 50 °C km^{-1}, which are values characteristic of volcanic arcs along convergent margins (Keary & Vine 1990), we obtain possible denudation rates of *c*. 0.24 mm a^{-1} to *c*. 0.12 mm a^{-1}, respectively. Rates within this range are consistent with uplift induced by shortening and thickening of the crust (Harrison *et al*. 1992), and are similar to the denudation rates that Goodge & Dallmeyer (1996) reported for the central Transantarctic Mountains.

Consideration of geochemical and geological data suggests that the Liv Group was deposited in an extensional rift setting proximal to an active Cambrian volcanic arc along a subducting margin (Borg *et al*. 1990; Stump 1995; Wareham *et al*. 2001). Interpretation of the Liv Group as a suprasubduction type basin has merit because it explains the presence of fossiliferous marine limestones (Rowell *et al*. 1997; Encarnación *et al*. 1999), bimodal volcanic rocks (Borg *et al*. 1990; Borg & DePaolo 1991; Stump 1995; Wareham *et al*. 2001), and plutons with a volcanic-arc geochemical signature (Borg *et al*. 1990; Borg & DePaolo 1991). On the basis of a modern-day analogue, Wareham *et al*. (2001) considered the *c*. 515 Ma basalts in the Liv Group to have been produced close to the axis of an intra-arc or back-arc rift system, and the 525 Ma silicic rocks of the Wyatt and Ackerman formations (which they included with the Liv Group) to have formed along the rift shoulder. We concur that deposition of the Liv Group in the Shackleton Glacier area probably occurred in an extensional basin(s) associated with subduction-related arc magmatism in the southern Transantarctic Mountains. Recent work suggests that the arc system may have been part of a larger collage of arcs (e.g. the Ellsworth Mountains and Bowers terranes) based on the similarity of isotopic age provinces, deformation timing, and Early to Mid-Cambrian volcanic–sedimentary successions among these blocks (Vennum *et al*. 1992; Borg & DePaolo 1994; Encarnación & Grunow 1996; Rowell *et al*. 1997; Duebendorfer & Rees 1998; Curtis *et al*. 1999; Grunow & Encarnación 2000*b*; Curtis 2001). It may be that the palaeo-Pacific margin of Gondwana was similar to the present Pacific–Eurasian plate boundary, with a complicated mix of multiple fringing arcs and subduction systems (Goodge *et al*. 1993; Grunow & Encarnación 2000*b*). We propose that post-505 Ma convergence across the arc system caused deformation of plutons and the inversion of basins in the Shackleton Glacier area. Left-oblique convergence, and thus transpressive deformation, may have ultimately been related to left-oblique plate subduction (Goodge *et al*. 1993; Encarnación & Grunow 1996), but our structural data do not constrain plate kinematics during this event.

On a regional scale, basin closure in the Shackleton Glacier area produced a structural belt of north- to NW-trending shear zones, folds and associated cleavage that trend at an oblique angle to the orogen (Fig. 1). Considering that the oblique structural grain of the belt coincides with a boundary in the Ross orogen that separates markedly different stratigraphic packages and isotopic patterns of plutons, we propose that the regional trend of these structures was inherited from the original shape of the basin(s) in which they formed. This proposal is supported by field and analogue model studies (Breen *et al*. 1989; Macedo & Marshak 1999), which indicate that the map-view shape of faults and related folds is strongly influenced by the shape of continental margins and blocks that become involved in collision zones. In other words, structural belts in the Ross orogen were effectively wrapped around the promonotories and embayments of marginal basins and blocks, as is the case for curves that developed in the Delamarian orogen, the northern extension of the Ross orogenic belt in Australia (Marshak & Flottmann 1996). The SWEAT hypothesis notwithstanding (i.e. East Antarctica was connected to Laurentia in the Late Precambrian; Dalziel 1991; Moores 1991; Stump 1992; Goodge 2002), the curvature of the orogen may provide a clue to the overall shape of the Neoproterozoic rift margin of East Antarctica (Brookfield 1993).

Conclusions

Our results provide the first kinematic evidence for transpressive deformation of supracrustal rocks in the southern Transantarctic Mountain sector of the Ross orogen. Goodge *et al*. (1993) documented deep-seated sinistral transpressive deformation (>25 km) beginning at *c*. 540 Ma in the central Transantarctic Mountains, and here we have documented kinematically compatible deformation as young as 505 Ma. Uplift and orogenic cooling appears to have begun at *c*. 500–490 Ma. Thus, the southern and central Transantarctic Mountain sectors of the Ross orogen may have been under a similar tectonic regime for *c*. 40 Ma. Considering the volcanic arc affinities of basement rocks in the southern Transantarctic Mountains, a likely tectonic model for deformation in the Shackleton Glacier region is one of left-oblique convergence across a subduction-related volcanic arc system.

This work was funded by NSF grant OPP-9317673 to A.G., NSF grant OPP-9527319 to A.G. and T.P., and NSF grant OPP-9615398 to J.E. We thank R. Allmendinger for providing his stereonet program. C. Demosthenous provided reviews that clarified drafts of this manuscript. R. Bresnahan helped in conducting shear-sense analyses. We thank K. Foland and F. Hubacher for advice and assistance with the argon analyses. We are also grateful for helpful reviews by J. Goodge, A. Rowell, M. Curtis and E. Stump.

References

Alexander, E.C. Jr, Michelson, G.M. & Lanphere, M.A. 1978. MMhb-1: a new $^{40}Ar/^{39}Ar$ dating standard. *In:* Zartman, R.E. (ed.) *Short Papers of the Fourth International Conference, Geochronology, Cosmochronology, Isotope Geology*. US Geological Survey, Open-File Report, **78-701**, 6–8.

Allibone, A. & Wysoczanski, R. 2002. Initiation of magmatism during the Cambrian–Ordovician Ross orogeny in southern Victoria Land, Antarctica. *Geological Society of America Bulletin*, **114**, 1007–1018.

Baldwin, S.L., Fitzgerald, P.G. & Swindle, T.D. 1995. $^{40}Ar/^{39}Ar$ constraints on the thermal history of basement rocks in the Scott Glacier region of the Transantarctic Mountains. *In:* Ricci, C.A. (ed.) *VII International Symposium*

on Antarctic Earth Sciences. Terra Antartica, Siena, 16.

Baldwin, S.L., Fitzgerald, P.G., Li, B. & Miller, S.R. 1999. Thermal evolution of the Transantarctic Mountains in the Shackleton Glacier area. *In:* Skinner, D.N.B. (ed.) *VIII International Symposium on Antarctic Earth Sciences*. Royal Society of New Zealand, Wellington, 33.

Barrett, P.J. 1965. Geology of the area between the Axel Heiberg and Shackleton Glaciers, Queen Maud Mountains, Antarctica. *New Zealand Journal of Geology and Geophysics*, **8**, 344–370.

Blanckenburg, F.V., Villa, I.M., Baur, H., Morteani, G. & Steiger, R.H. 1989. Time calibration of a *P–T* path from the Tauern window Eastern Alps: the problem of closure temperature. *Contributions to Mineralogy and Petrology*, **101**, 1–11.

Borg, S.G. & DePaolo, D.J. 1991. A tectonic model of the Antarctic Gondwana margin with implications for southeastern Australia: isotopic and geochemical evidence. *Tectonophysics*, **196**, 339–358.

Borg, S.G. & DePaolo, D.J. 1994. Laurentia, Australia, and Antarctica as a Late Proterozoic supercontinent: constraints from isotopic mapping. *Geology*, **22**, 307–310.

Borg, S.G., Stump, E., Chappell, M.T., McCulloch, M.T., Wyborn, D., Armstrong, R.L. & Holloway, J.R. 1987. Granitoids of northern Victoria Land, Antarctica: implications of chemical and isotopic variations to regional crustal structure and tectonics. *American Journal of Science*, **287**, 127–169.

Borg, S.G., DePaolo, D.J. & Smith, B.M. 1990. Isotopic structure and tectonics of the central Transantarctic Mountains. *Journal of Geophysical Research*, **95**, 6647–6667.

Breen, N.A., Silver, E.A. & Roof, S. 1989. The Wetar back arc thrust belt, eastern Indonesia; the effect of accretion against an irregularly shaped arc. *Tectonics*, **8**, 85–98.

Brookfield, M. 1993. Neoproterozoic Laurentia–Australia fit. *Geology*, **21**, 683–686.

Bürgmann, R. 1991. Transpression along the southern San Andreas fault, Durmid Hill, California. *Tectonics*, **10**, 1152–1163.

Cook, Y.A. & Craw, D. 2001. Amalgamation of disparate crustal fragments in the Walcott Bay–Foster Glacier area, South Victoria Land, Antarctica. *New Zealand Journal of Geology and Geophysics*, **44**, 403–416.

Curtis, M.L. 1997. Gondwanian age dextral transpression and spatial kinematic partitioning within the Heritage Range, Ellsworth Mountains, West Antarctica. *Tectonics*, **16**, 172–181.

Curtis, M.L. 2001. Tectonic history of the Ellsworth Mountains, West Antarctica: reconciling a Gondwana enigma. *Geological Society of America Bulletin*, **113**, 939–958.

Curtis, M.L., Leat, P.T., Riley, T.R., Storey, B.C., Millar, I.L. & Randall, D.E. 1999. Middle Cambrian volcanism in the Ellsworth Mountains: implications for palaeo-Pacific margin tectonics. *Tectonophysics*, **304**, 275–299.

Dalziel, I.W.D. 1991. Pacific margins of Laurentia and East Antarctica–Australia as a conjugate rift pair: evidence and implications for an Eocambrian supercontinent. *Geology*, **19**, 598–601.

DePaolo, D.J. 1996. High resolution Sm–Nd mineral geochronology of magmatism and metamorphism in the Transantarctic Mountains. *Geological Society of America, Abstracts with Programs*, **28**, A61.

Dodson, M.H. 1979. Theory of cooling ages. *In:* Jager, E. & Hunziker, H.C. (eds) *Lectures in Isotope Geology.* Springer, Berlin, 194–202.

Duebendorfer, E.M. & Rees, M.N. 1998. Evidence for Cambrian deformation in the Ellsworth–Whitmore Mountains terrane, Antarctica: stratigraphic and tectonic implications. *Geology*, **26**, 55–58.

Encarnación, J. & Grunow, A. 1996. Changing magmatic and tectonic styles along the paleo-Pacific margin of Gondwana and the onset of early Paleozoic magmatism in Antarctica. *Tectonics*, **15**, 1325–1341.

Encarnación, J., Rowell, A.J. & Grunow, A. 1999. A U–Pb age for the Cambrian Taylor Formation, Antarctica: implications for the Cambrian time scale. *Journal of Geology*, **107**, 497–504.

Fitzgerald, P.G. 1992. The Transantarctic Mountains of southern Victoria Land: the application of apatite fission track analysis to a rift shoulder uplift. *Tectonics*, **11**, 634–662.

Goodge, J.W. 1997. Latest Neoproterozoic basin inversion of the Beardmore Group, central Transantarctic Mountains, Antarctica. *Tectonics*, **16**, 682–701.

Goodge, J.W. 2002. From Rodinia to Gondwana: supercontinent evolution in the Transantarctic Mountains. *Royal Society of New Zealand Bulletin*, **35**, 61–74.

Goodge, J.W. & Dallmeyer, R.D. 1992. $^{40}Ar/^{39}Ar$ mineral age constraints on the Paleozoic tectonothermal evolution of high-grade basement rocks within the Ross Orogen, central Transantarctic Mountains. *Journal of Geology*, **100**, 91–106.

Goodge, J.W. & Dallmeyer, R.D. 1996. Contrasting thermal evolution within the Ross Orogen, Antarctica; evidence from mineral $^{40}Ar/^{39}Ar$ ages. *Journal of Geology*, **104**, 435–458.

Goodge, J.W., Hansen, V.L., Peacock, S.M., Smith, P.K. & Walker, N.W. 1993. Kinematic evolution of the Miller Range shear zone, central Transantarctic Mountains, and implications for Neoproterozoic to early Paleozoic tectonics of the East Antarctic margin of Gondwana. *Tectonics*, **12**, 1460–1478.

Grindley, G.W. & Laird, M.G. 1969. Geology of the Shackleton Coast. *American Geographical Society, Antarctic Map Folio Series*, folio 12, plate 14.

Grunow, A.M. & Encarnación, J. 2000a. Cambro-Ordovician paleomagnetic and geochronologic data from southern Victoria Land, Antarctica: revision of the Gondwana Apparent Polar Wander Path. *Geophysical Journal International*, **141**, 391–400.

Grunow, A.M. & Encarnación, J. 2000b. Allochthonous terranes or true polar wander: new data from the Scott Glacier area, Antarctica. *Tectonics*, **19**, 168–181.

Grunow, A.M., Encarnación, J., Paulsen, T. & Rowell, A.J. 1996. New geologic constraints on basement rocks from the Shackleton Glacier region. *Antarctic Journal of the United States Review*, **31**, 18–19.

Harland, W.B. 1971. Tectonic transpression in Caledonian Spitzbergen. *Geological Magazine*, **108**, 27–42.

Harrison, T.M. 1981. Diffusion of ^{40}Ar in hornblende. *Contributions to Mineralogy and Petrology*, **78**, 324–331.

Harrison, T.M., Copeland, P., Kidd, W.S.F. & Yin, A. 1992. Raising Tibet. *Science*, **255**, 1633–1670.

Jones, S. 1997. Contrasting structural styles during polyphase granitoid intrusion, South Victoria Land, Antarctica. *New Zealand Journal of Geology and Geophysics*, **40**, 237–251.

Isbell, J.L. 1999. The Kukri Erosion surface; a reassessment of its relationship to rocks of the Beacon Supergroup in the central Transantarctic Mountains, Antarctica. *Antarctic Science*, **11**, 228–238.

Keary, P. & Vine, F.J. 1990. *Global Tectonics*. Blackwell Scientific, Oxford.

Kirkwood, D. 1995. Strain partitioning and progressive deformation history in a transpressive belt, northern Appalachians. *Tectonophysics*, **241**, 15–34.

Kirkwood, D., Malo, M., St-Julien, P. & Therrien, P. 1995. Vertical and fold-axis parallel extension within a slate belt within a transpressive setting, northern Appalachians. *Journal of Structural Geology*, **17**, 329–343.

Kleinschmidt, G., Buggisch, W. & Flottmann, T. 1992. Compressional evidence for the early Paleozoic Ross orogen—evidence from Victoria Land and the Shackleton Range. *In:* Yoshida, Y., Kaminuma, K. & Shrirashi, K. (eds) *Recent Progress in Antarctic Earth Science*. Terra, Tokyo, 227–233.

Lafrance, B. 1989. Structural evolution of a transpression zone in north central Newfoundland. *Journal of Structural Geology*, **11**, 705–716.

Macedo, J. & Marshak, S. 1999. Controls on the geometry of fold–thrust belt salients. *Geological Society of America Bulletin*, **111**, 1808–1822.

Mancktelow, N.S. & Pavlis, T.L. 1994. Fold–fault relationships in low-angle detachment systems. *Tectonics*, **13**, 668–685.

Marshak, S. & Flottmann, T. 1996. Structure and origin of the Fleurieu and Nackara arcs in the Adelaide fold–thrust belt, South Australia: salient and recess development in the Delamerian Orogen. *Journal of Structural Geology*, **18**, 891–908.

McGregor, V.R. 1965. Geology of the area between the Axel Heiberg and Shackleton Glaciers, Queen Maud Range, Part 1—basement complex, structure and glacial geology. *New Zealand Journal of Geology and Geophysics*, **8**, 314–343.

McGregor, V.R. & Wade, F.A. 1969. Geology of the Western Queen Maud Mountains. *American Geographical Society, Antarctic Map Folio Series*, folio 12, map 15.

Mellish, S.D., Cooper, A.F. & Walker, N.W. 2002. Panorama Pluton: a composite gabbro–monzodiorite early Ross Orogeny intrusion in southern Victoria Land, Antarctica. *Royal Society of New Zealand Bulletin*, **35**, ;129–141.

Miller, S.R., Fitzgerald, P.G. & Baldwin, S.L. 2001. Structure and kinematics of the Central Transantarctic Mountains: constraints from structural geology and geomorphology near Cape Surprise. *Terra Antartica*, **8**, 11–24.

Mirsky, A. 1969. Geology of the Ohio Range–Liv Glacier area. *American Geographical Society, Antarctic Map Folio Series*, folio 12, map 16.

Moores, E.M. 1991. The southwest U.S.–East Antarctic (SWEAT) connection: a hypothesis. *Geology*, **19**, 425–428.

Myrow, P.M., Pope, M.C., Goodge, J.W., Fischer, W. & Palmer, A.R. 2002. Depositional history of pre-Devonian strata and timing of Ross orogenic tectonism in the central Transantarctic Mountains, Antarctica. *Geological Society of America Bulletin*, **114**, 1070–1088.

Passchier, C.W. & Trouw, R.A.J. 1996. *Microtectonics*. Springer, Berlin.

Platt, J.P. 1993. Mechanics of oblique convergence. *Journal of Geophyiscal Research*, **98**, 16239–16256.

Price, N.J. & Cosgrove, J.W. 1990. *Analysis of Geologic Structures*. Cambridge University Press, Cambridge.

Read, S.E. & Cooper, A.F. 1999. New U–Pb isotopic age determinations from plutons in the Ross Orogen, southern Victoria Land, Antarctica. *In:* Skinner, D.N.B. (ed.) *8th International Symposium on Antarctic Earth Sciences; Programme and Abstracts*. Royal Society of New Zealand, Wellington, 262.

Renne, P.R., Deino, A.L. & Walter, R.C. *et al.* 1994. Intercalibration of

astronomical and radioisotopic time. *Geology*, **22**, 783–786.

Rocchi, S., Tonarini, S., Armienti, P., Innocenti, F. & Manetti, P. 1997. Geochemical and isotopic structure of the early Palaeozoic active margin of Gondwana in northern Victoria Land, Antarctica. *Tectonophysics*, **284**, 261–281.

Rowell, A.J. & Rees, M.N. 1989. Early Paleozoic history of the upper Beardmore Glacier area: implications for a major Antarctic structural boundary within the Transantarctic Mountains. *Antarctic Science*, **1**, 249–260.

Rowell, A.J., Rees, M.N. & Evans, K.R. 1992. Evidence of major Middle Cambrian deformation in the Ross orogen, Antarctica. *Geology*, **20**, 31–34.

Rowell, A.J., Rees, M.N., Duebendorfer, E.M., Wallin, E.T., Van Schmus, W.R. & Smith, E.I. 1993. An active Neoproterozoic margin: evidence from the Skelton Glacier area, Transantarctic Mountains. *Journal of the Geological Society, London*, **150**, 677–682.

Rowell, A.J., Gonzales, D.A., McKenna, L.W., Evans, K.R., Stump, E. & Van Schmus, W.R. 1997. Lower Paleozoic rocks in the Queen Maud Mountains: revised ages and significance: Antarctic geology and geophysics. *The Antarctic Region: Geological Evolution and Processes*. Terra Antarctica Publication, Siena, 201–207.

Rowell, A.J., Van Schmus, W.R., Storey, B.C., Fetter, A.H. & Evans, K.R. 2001. Latest Neoproterozoic to mid-Cambrian age for the main deformation phases of the Transantarctic Mountains: new stratigraphic and isotopic constraints from the Pensacola Mountains, Antarctica. *Journal of the Geological Society, London*, **158**, 295–308.

Sanderson, D.J. & Marchini, W.R.D. 1984. Transpression. *Journal of Structural Geology*, **6**, 449–458.

Sylvester, A.G. 1988. Strike-slip faults. *Geological Society of America Bulletin*, **100**, 1666–1703.

Stump, E. 1974. Volcanic rocks of the Early Cambrian Taylor Formation, central Transantarctic Mountains. *Antarctic Journal of the United States*, **9**, 228–229.

Stump, E. 1981. Structural relationships in the Duncan Mountains, central Transantarctic Mountains, Antarctica. *New Zealand Journal of Geology and Geophysics*, **24**, 87–93.

Stump, E. 1982. The Ross Supergroup in the Queen Maud Mountains. *In:* Craddock, C. (ed.) *Antarctic Geoscience*. University of Wisconsin Press, Madison, WI, 565–569.

Stump, E. 1985. Stratigraphy of the Ross Supergroup, central Transantarctic Mountains. *Antarctic Research Series*, **36**, 225–274.

Stump, E. 1992. The Ross Orogen of the Transantarctic Mountains in light of the Laurentia–Gondwana split. *GSA Today*, **2**, 1–31.

Stump, E. 1995. *The Ross Orogen of the Transantarctic Mountains*. Cambridge University Press, Cambridge.

Stump, E., Edgerton, D.G. & Korsch, R.J. 2002. Geologic relationships at Cotton Plateau, Nimrod Glacier area, bearing on the tectonic development of the Ross Orogen, Transantarctic Mountains, Antarctica. *Terra Antartica*, **9**, 3–18.

Van Schmus, W.R., McKenna, L.W., Gonzales, D.A., Fetter, A.H. & Rowell, A.J. 1997. *In:* Ricci, C.A. (ed.) *The Antarctic Region: Geological Evolution and Processes*. Terra Antarctica Publication, Siena, 187–200.

Vennum, W.R., Gizycki, P., Samsonov, V.V., Markovich, A.G. & Pankhurst, R.J. 1992. Igneous petrology and geochemistry of the southern Heritage Range, Ellsworth Mountains, West Antarctica. *Geological Society of America Bulletin*, **170**, 295–324.

Vogel, M.B., Ireland, T.R. & Weaver, S.D. 2002. The multistage history of the Queen Maud Batholith, La Gorce Mountains, central Transantarctic Mountains. *Royal Society of New Zealand Bulletin*, **35**, 153–159.

Wade, F.A. 1974. Geological surveys of Marie Byrd Land and the central Queen Maud Range. *Antarctic Journal of the United States*, **9**, 241–242.

Wade, F.A. & Cathey, C.A. 1985. Geology of the basement complex, western Queen Maud Mountains, Antarctica. *Antarctic Research Series*, **36**, 225–274.

Wade, F., Yeats, V.L., Everett, J.R., Greenlee, D.W., LaPrade, K.E. & Shenk, J.C. 1965. *The Geology of the Central Queen Maud Range, Transantarctic Mountains, Antarctica*. Texas Technical College Antarctic Research Report Series, **65-1**.

Wareham, C.D., Stump, E., Storey, B.C., Millar, I.L. & Riley, T.R. 2001. Petrogenesis of the Cambrian Liv Group, a bimodal volcanic rock suite from the Ross Orogen, Transantarctic Mountains. *Geological Society of America Bulletin*, **113**, 360–372.

Received 7 April 2003; revised typescript accepted 5 February 2004.
Scientific editing by Haakon Fossen